

Earthquake connections on mapped California faults ranked by calculated static linking stresses

by Tom Parsons, Edward H. Field, Morgan T. Page, and Kevin Milner

Abstract. A method to discriminate amongst a wide range of possible ruptures within a large fault system is explored. We hypothesize that many of the conditions favoring earthquake rupture propagation can be simulated using a static stress change approximation. Such an approach lacks inertial effects inherent in a full dynamic simulation, but does capture many of the empirical observations drawn from past ruptures, such as continuity of rake, strike, and distance across gaps or stepovers. We made calculations for a test region in northern California and found the method does provide a quantitative basis for ranking possible ruptures with localized fault systems. However, application of the method to rank all ruptures uniformly throughout California will require a very regularized characterization of fault subsections.

Introduction

Fault-based earthquake forecasts require decisions about the connectivity of the fault network. For example, can future ruptures propagate through sharp bends, jump across observed fault interruptions, and/or stepovers? The critical offset distance for an earthquake to jump through a stepover is thought to be about 3-5 km, based on observations and numerical modeling (Barka and Kandinsky-Cade, 1988; Harris, 1992; Harris and Day, 1993; 1999; Kase and Kuge,

1998; Lettis et al., 2002; Wesnousky, 2008; Ogelsby, 2008; Elliott et al., 2009; Lozos et al., 2011). However, these same investigators note that rupture continuity and branching is situational, depending on a variety of factors including: (1) whether the stepover is releasing or restraining, (2) the relative orientations and stress states on faults, (3) rake variations, and (4) slip distribution within the rupture. Therefore a simple rule-of-thumb, such as fault separation distance, may not be a sufficient criterion for decision making.

Generally, fault-based earthquake forecasts rely on geological segmentation (e.g., McCann et al., 1979; Working Group on California Earthquake Probabilities (WGCEP), 1988; 1990; 1995; 2003; Frankel et al., 2002; Earthquake Research Committee, 2005; Romeo, 2005; Petersen et al., 2008; Field et al., 2009), which defines minimum/maximum rupture extents by identifying geometrical features of fault zones thought to arrest ruptures. However, as we observe more large earthquakes in detail, we note surprising involvement of relatively minor (and sometimes previously unrecognized) faults in combination with major faults. For example, the 2002 $M=7.9$ Denali earthquake “began with thrusting on the previously unrecognized Susitna Glacier fault, continued with right-slip on the Denali fault, then took a right step and continued with right-slip on the Totschunda fault” (Eberhart-Phillips et al., 2003). The 2008 $M=8.0$ Wenchuan earthquake occurred on three distinct and subparallel surface ruptures (Li et al., 2008). Neither of these exact earthquakes would likely have been included in a segmented, fault source forecast. Computationally intensive methods exist to consider all possible ruptures within complex fault systems (e.g., Field and Page, 2011), however geologically-based decision making regarding branching and stepping ruptures on a case-by-case basis for thousands of fault combinations is impractical, if not impossible.

If we want to create an earthquake rupture forecast that considers all possible fault combinations, we require a basis for ranking possible ruptures that is as sensitive as practical to specific geometries throughout a fault system, and that can be consistently applied in an automated way. While considering all possible ruptures, we seek a means to rank them from least to most probable. Ideally, fully dynamic earthquake simulations would be calculated for every rupture; however at present, the computational and parameter demands of this exceed capability.

In this paper we introduce the concept of static linking stresses. This is an exploration into the use of static stress transmission as a proxy for dynamic rupture propagation. The static solution lacks the inertial components of a fully dynamic solution, but can capture many of the other features that promote or inhibit rupture propagation from one fault section to another. These include distance between sections, overlap, relative rakes, dips, and changes in strike. We therefore rank proposed earthquake ruptures by their links as a means of answering the question, does this particular proposed junction or branch make more or less physical sense than another choice?

Method

An effective earthquake rupture forecast must specify the complete magnitude distribution that will affect a region as accurately as possible. This is generally accomplished with geological observations on fault geometry to identify likely rupture dimensions. Here we explore the idea that static stress transfer can capture and quantify the majority of these observations, while enabling consideration of massive numbers of possibilities. Coulomb stress change values are sensitive to distance, being much stronger with proximity. Thus the calculations may encompass

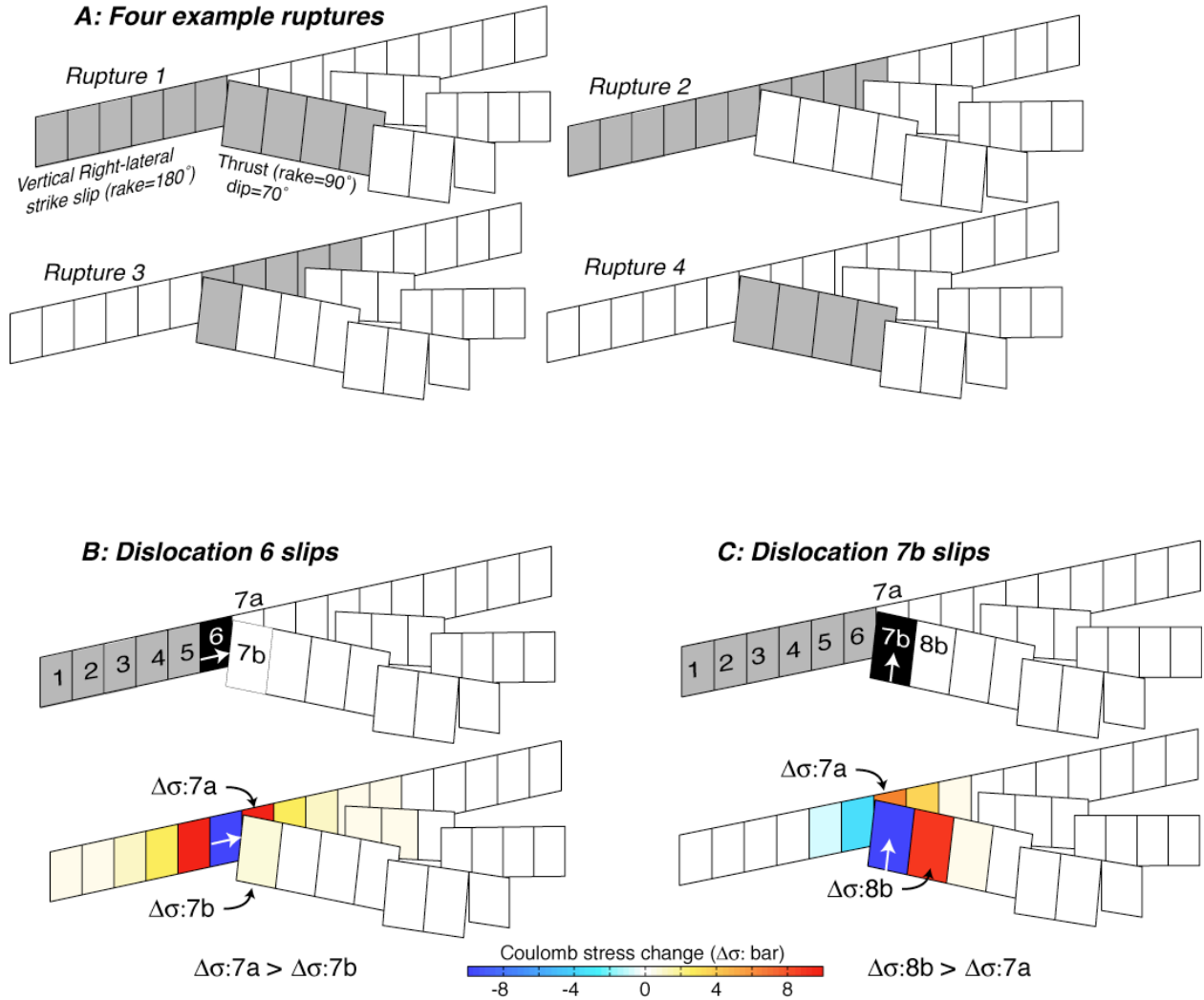


Figure 1. Example calculations. (a) Rectangles show fault subsections within four potential ruptures, which we would like to assess relative viability. The ruptures in these examples can branch between vertical strike-slip faults and dipping thrusts. In (b) dislocation number 6, which lies at a fault junction, slips 1 m. It causes a larger static stress change on subsection 7a than 7b, which would cause Rupture 2 to be more favored than Rupture 1 when all the linking stresses are averaged. In (c) dislocation number 7b is slipped, which increases stress at 8b more than at 7a, implying that Rupture 4 is more favored than Rupture 3, but only slightly. Slip at 7b puts dislocations 5 and 6 into a stress shadow, which implies that a potential rupture going the reverse direction on the strike-slip fault is not mechanically viable.

rule-of-thumb ideas about fault steps and gaps derived from empirical studies. Further, Coulomb stress change calculations are larger when stress is transferred to compatible rakes. For example, stress changes are negative between along-strike right-lateral and left-lateral fault subsections, but would be positive between a strike-slip and orthogonal thrust fault link that are appropriately located to accommodate tectonic strain (Figure 1). Thus static stress calculations can capture mechanically sensible fault junctions, and penalize those that, while lying within the observed 3-5 km distance criterion, are not mechanically viable. Other examples that are penalized are closely spaced, parallel subsections with the same rakes, because slip on one puts the other into a stress shadow.

Development of the Uniform California Earthquake Rupture Forecast (UCERF) includes cataloging all known active faults in California as seismic sources. These faults are broken into subsections that extend through the complete seismogenic thickness (typically 12-15 km; Field et al., 2009) and are ~half the seismogenic thickness in length (Figure 2). Each subsection has known or estimated dip and rake values assigned.

We begin with a list of possible ruptures from within the California fault model. A “possible” rupture means any combination of mapped fault subsections that is not specifically identified as impossible. We define three classes of ruptures as impossible; these are “full-circle” ruptures that start and stop at the same point, “U-turn” ruptures that reverse direction by taking a greater than 90° turn, and very long stepping ruptures that jump across distances in excess of 10 km. All other combinations are considered possible, though many may be very unlikely. The list of possible ruptures includes those that occur on a single defined fault as well as ones that branch onto other faults. The smallest ruptures in the model occupy two subsections; they then systematically include additional subsections up to the longest maximum extent possible. Each

fault branch or junction represents another series of possible ruptures, as every possible choice is explored out to maximum extent.

Subsection geometry and rake data are used to create an elastic dislocation model for each one with the methods of Okada (1992) and Simpson and Reasenberg (1994). Our goal is to rank every rupture in a relative way, so each source dislocation is assigned uniform slip of 1 m. A second complete set of dislocation models is made

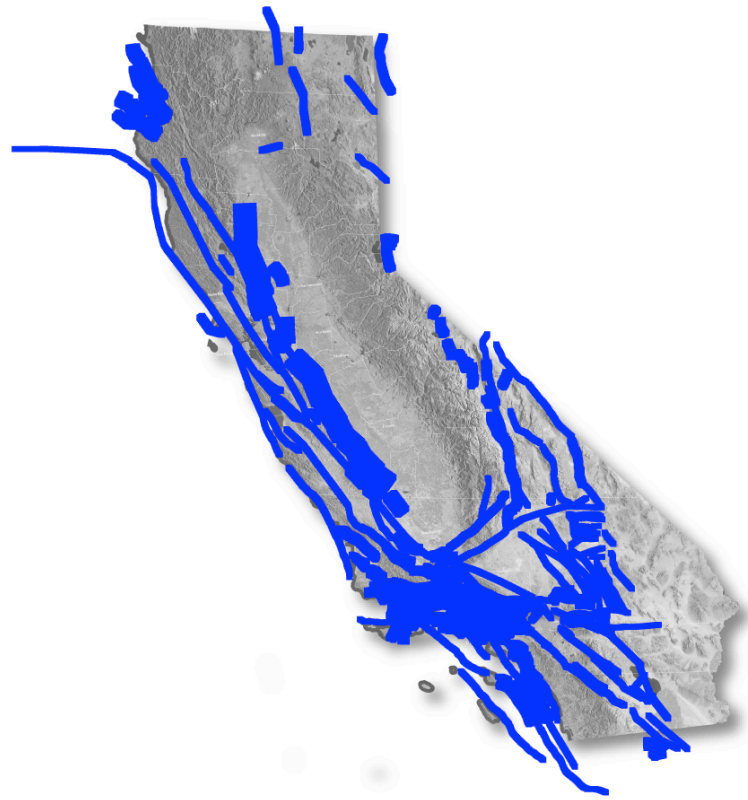


Figure 2. California mapped faults simplified into subsections.

from the fault database that are target dislocations upon which static stress changes can be resolved. Static stress change is calculated by solving for Coulomb failure stress ($\Delta\tau$) as $\Delta\tau \equiv |\Delta\bar{\tau}_f| + \mu(\Delta\sigma_n - \Delta p)$, where $\Delta\bar{\tau}_f$ is the change in shear stress on the receiver fault (set positive in the rake direction), μ is the coefficient of friction, $\Delta\sigma_n$ is the change in normal stress acting on the target fault (set positive for unclamping), and Δp is pore pressure change (neglected here). We use a constant friction coefficient of $\mu=0.5$ throughout the model, just as we use a constant slip of 1 m, because we are interested in direct comparison of different possible ruptures, and we want to treat them uniformly.

The geographic center is determined for each rupture, and the dislocation models for that rupture are projected into a local coordinate system using a Mercator projection in km. Coulomb stress changes are systematically calculated using each dislocation of the rupture as a source, while all other dislocations are targets. This creates a matrix of stress communications amongst the rupture. We are interested in links between adjacent subsections; for example, is a rupture more or less likely to move long a given pathway when there are many branching choices? Adjacency between subsections is a three-dimensional problem because dipping and curving faults may be closer at depth than they are on the surface. The stress change calculations solve this issue for us because they are so sensitive to proximity, falling off as a function of the cube root of distance. We therefore sort the matrix of stress change values largest to smallest.

For each potential rupture, we draw the highest-value links from the sorted list of stress change values without allowing any sources or targets to be repeated. This finds the most adjacent subsections and their linking stress changes, but does not allow any part of the proposed rupture to slip twice. Once the list of stress links of a rupture are gathered, we normalize by dividing the sum of the stress changes by the number of links (1 – number-of-subsections). Each

rupture then can be characterized by a single value that describes its continuity and rake consistency. Ruptures with long gaps and/or poorly aligned linking faults have a smaller mean linking stress than a more continuous version.

Applications, caveats, and sources of uncertainty

How should the linking stress be used? Can all ruptures be compared directly? For example, a long rupture with 100 subsection links might include just one long gap that produces one unfavorable stress change. Its signal is muted when averaged with the other 99 links, making comparison of this rupture with another in a completely different region or fault system problematic. However, comparison of this value with that from ruptures on the same fault, but that stop short of the gap, could provide useful ranking information.

As discussed above, Coulomb stress change calculations are very sensitive to the distance between source and target dislocations. Therefore, uncertainty related to mapped fault end points has important impact of the magnitude of calculated stress change. This uncertainty can be magnified as the dislocations are projected downdip, which of course is also affected by dip uncertainty. Expert geological assessments can provide informed weighting in settings where a fault end point might, for example, be mapped because of thin sedimentary cover, but the fault actually is thought to persist closer or even link directly with another. By comparison, another end point might be very well characterized in hard rock, leaving little doubt. The relative value of these observations would not be accommodated in a stress change calculation unless some quantified uncertainty was given.

Dynamic rupture simulations indicate important effects of preexisting stress distribution (Harris and Day, 1993; 1999) that can determine whether a rupture jumps onto a branching fault, or clears a stepover. Additionally, the distribution of slip within a rupture can affect whether a jump occurs or not (Ogelsby, 2008; Elliott et al., 2009). These important effects are not addressable with a static stress approach. A feature that is captured in moment-balanced models (Field et al., 2009) is the relative odds of ruptures jumping onto a lower slip rate fault vs. staying on a major fault, because their frequencies are governed by observed long-term slip rates.

Test Case Results

A subset region was used for feasibility testing that includes northern California faults (Figure 3). The subset region includes 20614 possible ruptures, each of which was assessed with linking stress calculations. In this section we present some example results from the calculations for examination. The potential ruptures range in inferred magnitude from $M=5.2$ to $M=8.2$, with the majority being large ruptures (Figure 4).

A key issue in earthquake forecasting is establishing the magnitude distribution affecting the region of interest, and the relative ability of ruptures to jump from fault to fault has an important influence on possible rupture areas. Certainly the magnitude distribution of possible ruptures (Figure 4) is unlike the observed for large regions, which follow the Gutenberg-Richter power law distribution. Balancing the earthquake rupture model against observed slip rates or plate motion rates can reduce the allowable number of the largest (hence most slip) events in the model.

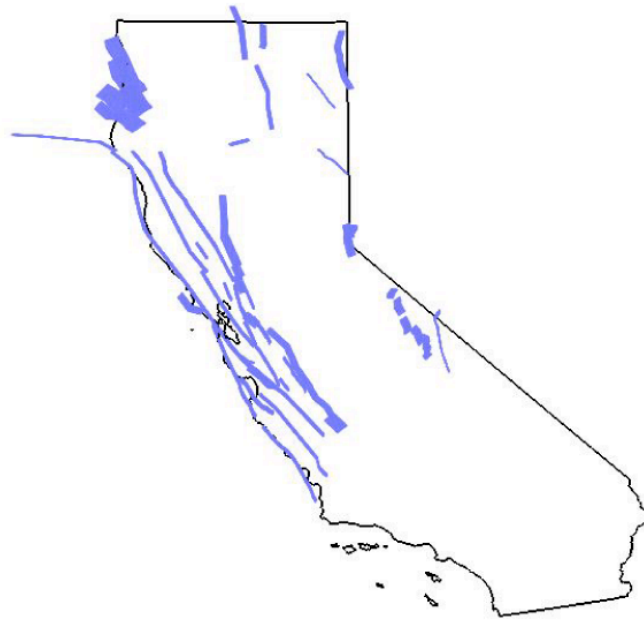


Figure 3. Test region in northern California/San Francisco Bay region. The faults and their subsections that were used in the method testing are shaded blue.

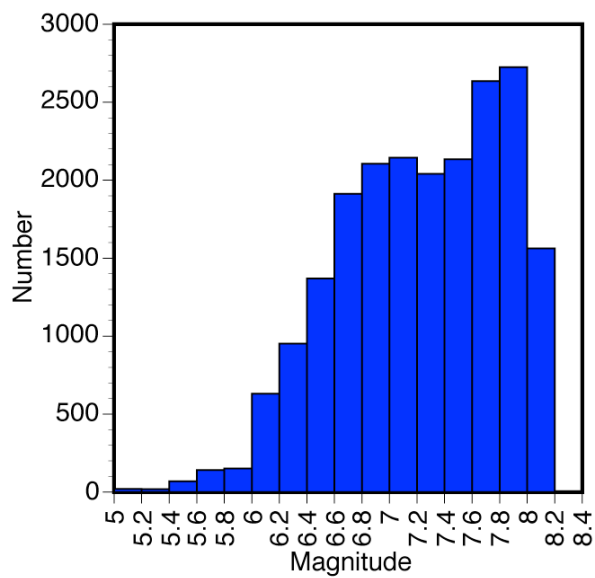


Figure 4. Magnitude distribution of possible ruptures from the test region in northern California/San Francisco Bay region shown in Figure 3. The distribution is weighted most heavily toward larger magnitudes.

We show an example calculation for two possible ruptures from Hayward-Calaveras fault system in the eastern San Francisco Bay region. The two ruptures have very similar magnitudes, but one involves a step from the Calaveras to the Hayward fault, while the other lies entirely on the Calaveras. Relatively small magnitude ($M=6.4$) ruptures are used for this comparison to minimize complications from other structural influences, like bends. As would be expected, we find that the continuous rupture has a higher mean linking stress than the jumping rupture by a factor greater than 5 (Figure 5). An equivalent magnitude Hayward-fault only rupture has more than double the mean linking stress of the jumping rupture (17.4 bars compared with 8.4).

This example illustrates a possible method for quantifying the likelihood that a rupture will branch onto an adjacent fault vs. remaining on a continuous fault. The stress values could be used as a relative ranking, or could be used to give proportional weight to different rupture scenarios. However, some normalization may be necessary before direct weighting could be employed; the example given in Figure 5 highlights an issue in that the section divisions have influence on the overall linking stress magnitudes. A continuous Calaveras fault rupture has a 45.8 bar mean linking stress compared with 17.4 bars for an equivalent south Hayward fault rupture, a result of larger linking shear stress changes. Thus while the ranks amongst jumping vs. continuous ruptures is correct, comparison between two continuous ruptures on two different faults is more difficult.

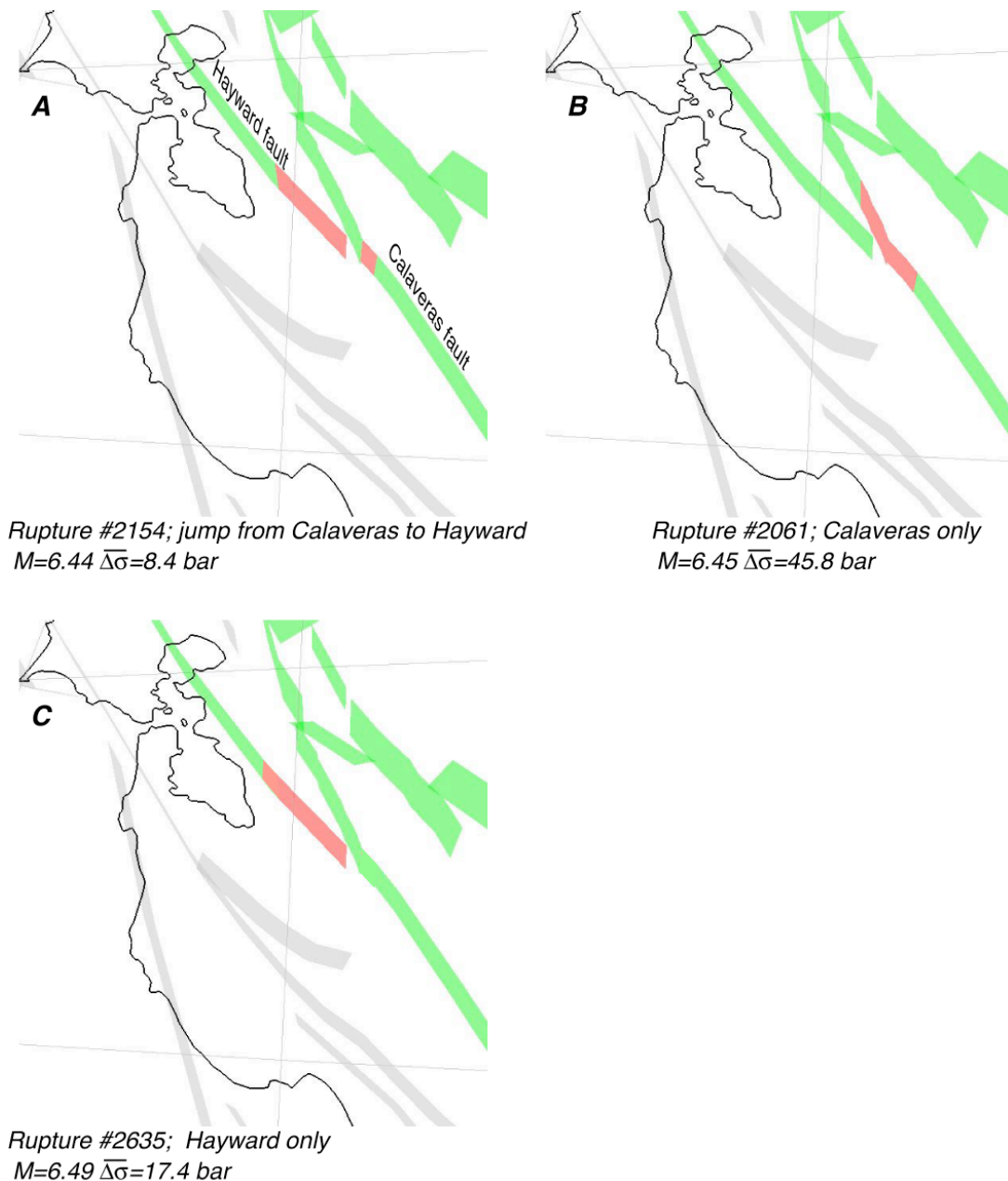


Figure 5. Example rupture ranking using linking stress in the San Francisco Bay region. In (a), a $M=6.44$ model rupture (shown by red shading) jumps from the Calaveras fault across a gap onto the south Hayward fault; the mean calculated linking stress for this rupture is 8.4 bars. In (b) an equivalent magnitude ($M=6.45$) rupture that is continuous on the Calaveras fault is shown, which has a mean linking stress of 45.8 bars, a factor 5.5 greater. In (c) the equivalent rupture is contained on the south Hayward fault, with has a mean linking stress of 17.4 bars.

No directivity is implied, the ruptures have the same linking stress whether they go from north to south or vice versa.

We give another example result taken from a circumstance where manual rupture prioritization would be very difficult, a series of imbricate thrust faults in the Mendocino region of northern California (Figure 6). The ratios between linking stresses for individual ruptures and the mean of the examples are used to rank their relative viability. In this example, a simple

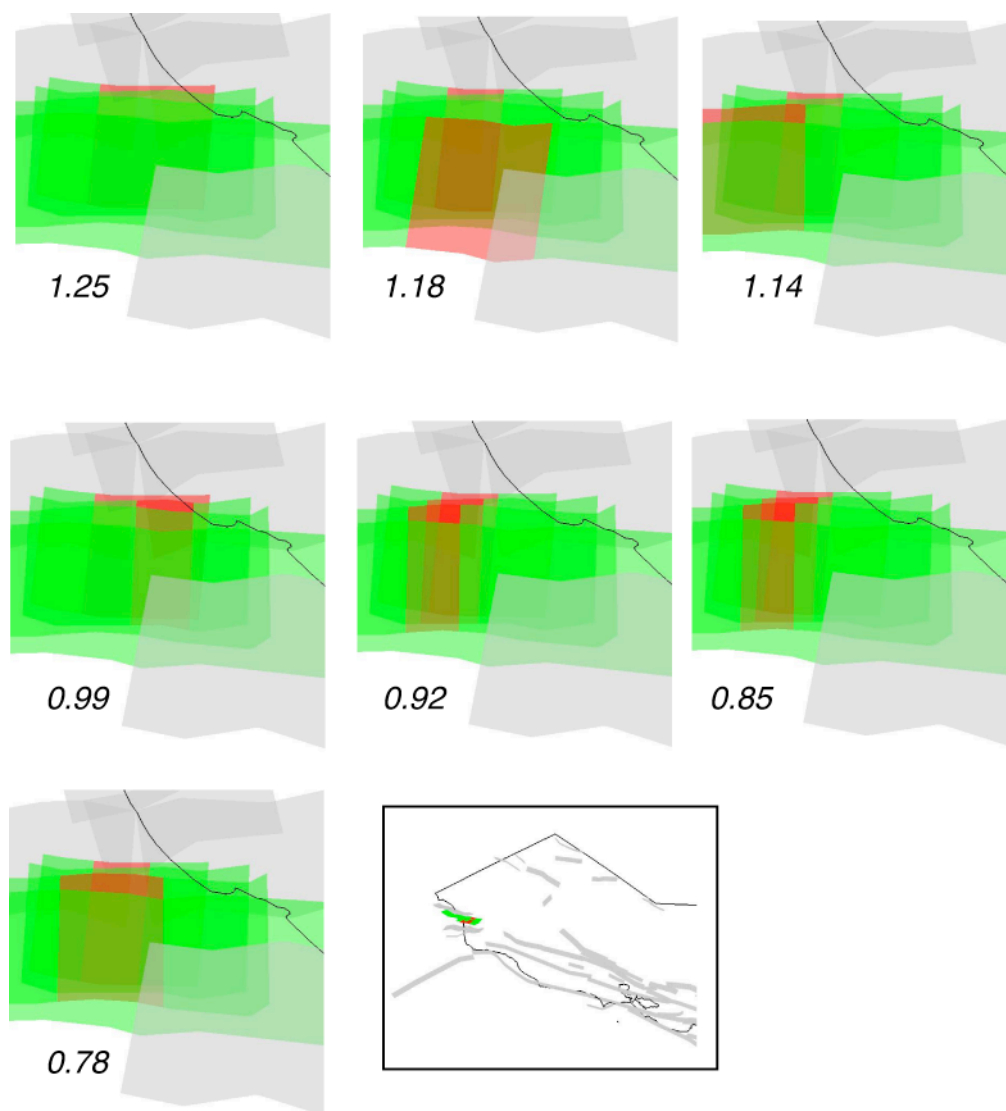


Figure 6. A series of possible ruptures within an imbricate thrust fault system in the Mendocino region of northern California (location shown in inset map). The

ruptures (shown in red) are ranked by taking the ratio between the linking stress calculated for each rupture to the mean of all the ruptures shown. The ruptures with less overlap tend to have higher linking stresses, and thus are calculated to be more viable.

continuous rupture that occurs on a single fault trace is compared with more complex, multi-fault ruptures. Surprisingly, some multi-fault ruptures are almost as highly ranked as the continuous example (Figure 6), which illustrates that details in fault geometry can potentially cause unexpected ruptures (something that mirrors observations). Other possible ruptures with significant overlap are ranked lower, as might be expected.

We lastly note a few observations from examining all the 20614 possible rupture ranks as a function of magnitude. The very highest ranked ruptures tend to be among the lowest magnitude considered ($M \sim 6.5$; Figure 7), though low magnitude ruptures are comparatively rare (Figure 4). The Appendix lists some of the highest ranked ruptures and their magnitudes (Table A1). Within the top 5000 ranked ruptures, there is a systematic decline in ranking with increasing magnitude. Rank dependence on magnitude is less clear amongst the lower ranked ruptures (rank < 5000; Figure 7). A future test of the method will involve a determination of moment balance solutions for rupture rates that can be compared with linking-stress based ranking.

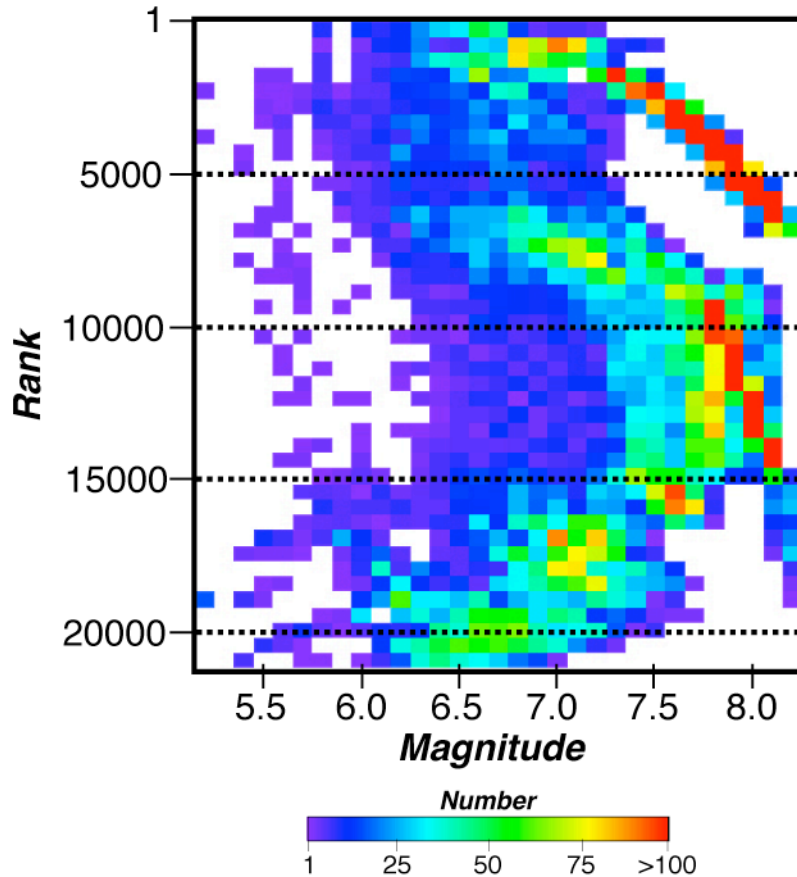


Figure 7. The distribution of possible ruptures as functions of their linking stress rank and magnitude. Top ranking is 1, and lowest is 20614. Despite the predominance of high magnitude ruptures studied (Figure 4), we find that most of the very highest ranked ruptures are $M \sim 6.5$. We note an apparent decline in rank as a function of magnitude within the top-5000 ranked ruptures.

Summary and Conclusions

Linking stress calculations appear most useful as a means of ranking ruptures in a local sense in terms of use within fault zones. We see consistent results in terms of ranking continuous ruptures vs. stepping junctions. However, we find also that a change in strike, or involvement with nearby subsections does not necessarily imply a lower rank. Calculations are very sensitive to details in fault subsection location, especially how the ends are defined. Therefore comparing solutions between fault zones where subsections are exactly adjacent of very nearly so with

different zones may require some normalization factors. We conclude the best use of the method is at decision points, such as fault junctions and branches that lie within the same system of faults.

Appendix

rupID	clusterID	rupInClustID	rank	linking_stress (Mpa)	num_subsects	M
505	0	505	1	1058.8	2	6.13
493	0	493	2	1051.2	2	6.13
3550	6	9	3	632.3	2	6.23
3546	6	5	4	632.3	2	6.23
481	0	481	5	529.8	3	6.30
494	0	494	6	525.7	3	6.30
4942	11	1147	7	440.9	2	5.77
4929	11	1134	8	440.9	2	5.77
4916	11	1121	9	417.1	3	5.94
4900	11	1105	10	392.9	2	5.77
4915	11	1120	11	392.7	2	5.77
468	0	468	12	356.6	4	6.43
482	0	482	13	353.2	4	6.43
3542	6	1	14	320.4	3	6.41
5336	14	201	15	317.4	2	6.02
3547	6	6	16	316.5	3	6.41
3551	6	10	17	316.2	3	6.41
4917	11	1122	18	282.1	4	6.07
4902	11	1107	19	277.9	4	6.07
454	0	454	20	268.2	5	6.52
469	0	469	21	266.3	5	6.52
4930	11	1135	22	226.7	3	5.94
4943	11	1148	23	223.7	3	5.94
439	0	439	24	214.7	6	6.60
455	0	455	25	214.5	6	6.60
4918	11	1123	26	213.2	5	6.16
3543	6	2	27	213.2	4	6.53
3548	6	7	28	213.0	4	6.53
4887	11	1092	29	212.0	5	6.16
4903	11	1108	30	211.7	5	6.16
3552	6	11	31	211.2	4	6.53
4885	11	1090	32	200.2	3	5.94
4901	11	1106	33	196.8	3	5.94
423	0	423	34	180.0	7	6.67
440	0	440	35	178.8	7	6.67
4871	11	1076	36	171.6	6	6.24
4919	11	1124	37	170.9	6	6.24
4888	11	1093	38	170.8	6	6.24
4904	11	1109	39	170.7	6	6.24

4920	11	1125	40	163.7	7	6.31
3549	6	8	41	160.4	5	6.63
5306	14	171	42	160.2	3	6.20
3544	6	3	43	159.7	5	6.63
5337	14	202	44	159.0	3	6.20
406	0	406	45	154.2	8	6.73
4944	11	1149	46	153.3	4	6.07
4931	11	1136	47	153.3	4	6.07
424	0	424	48	153.3	8	6.73
4945	11	1150	49	146.8	5	6.16
4872	11	1077	50	145.1	7	6.31
4889	11	1094	51	144.4	7	6.31
4854	11	1059	52	143.0	7	6.31
4905	11	1110	53	142.6	7	6.31
4921	11	1126	54	141.2	8	6.37
4906	11	1111	55	140.4	8	6.37
4886	11	1091	56	135.5	4	6.07
388	0	388	57	134.8	9	6.78
4869	11	1074	58	134.6	4	6.07
407	0	407	59	134.1	9	6.78
3545	6	4	60	127.9	6	6.71
4975	11	1180	61	127.2	2	5.77
4984	11	1189	62	127.2	2	5.77
4873	11	1078	63	124.5	8	6.37
4200	11	405	64	124.5	2	5.77
4240	11	445	65	124.5	2	5.77
4891	11	1096	66	124.4	9	6.42
4855	11	1060	67	124.4	8	6.37
4890	11	1095	68	123.8	8	6.37
4836	11	1041	69	123.6	8	6.37
4907	11	1112	70	123.6	9	6.42
4922	11	1127	71	123.6	9	6.42
389	0	389	72	119.9	10	6.83
369	0	369	73	119.8	10	6.83
4946	11	1151	74	118.7	6	6.24
4933	11	1138	75	117.4	6	6.24
4932	11	1137	76	115.0	5	6.16
4875	11	1080	77	111.6	10	6.46
4892	11	1097	78	111.2	10	6.46
4923	11	1128	79	111.1	10	6.46
4908	11	1113	80	109.8	10	6.46
4837	11	1042	81	109.8	9	6.42
4874	11	1079	82	109.6	9	6.42
4856	11	1061	83	109.0	9	6.42
370	0	370	84	108.7	11	6.88
349	0	349	85	108.7	11	6.88
4817	11	1022	86	108.1	9	6.42
5307	14	172	87	107.3	4	6.33
5338	14	203	88	107.3	4	6.33

5275	14	140	89	107.1	4	6.33
4870	11	1075	90	104.3	5	6.16
4852	11	1057	91	102.9	5	6.16
4876	11	1081	92	101.0	11	6.51
4947	11	1152	93	100.9	7	6.31
4858	11	1063	94	100.5	11	6.51
4893	11	1098	95	100.2	11	6.51
4909	11	1114	96	100.1	11	6.51
4924	11	1129	97	100.1	11	6.51
328	0	328	98	100.0	12	6.92
4934	11	1139	99	99.0	7	6.31

Table A1. A list of the top 100 ranked ruptures. The ruptures are organized into geographic clusters. Thus rankings can also be associated with clusters. The top ranked ruptures are all less than $M=7$.

References

- Barka, A. A., and K. Kandinsky-Cade (1988). Strike-slip fault geometry in Turkey and its influence on earthquake activity, *Tectonics*, **7**, 663-684.
- Earthquake Research Committee (2005). Comprehensive study of probabilistic seismic hazard map for Japan. Tokyo, Japan: Headquarters for Earthquake Research Promotion, 125 pp.
- Eberhart-Phillips, D., Haeussler, P.J., Freymueller, J.T., Frankel, A.D., Rubin, C.M., Craw, P., Ratchkovski, N.A., Anderson, G., Carver, G.A., Crone, A.J., Dawson, T.E., Fletcher, H., Hansen, R., Harp, E.L., Harris, R.A., Hill, D.P., Hreinsdóttir, S., Jibson, R.W., Jones, L.M., Kayen, R., Keefer, D.K., Larsen, C.F., Moran, S.C., Personius, S.F., Plafker, G., Sherrod, B., Sieh, K., Sitar, N., Wallace, W.K. (2003). The 2002 Denali fault earthquake, Alaska: A large magnitude, slip-partitioned event, *Science*, **300**, 1113-1118. DOI: 10.1126/science.1082703
- Elliott, A. J., J. F. Dolan, and D. D. Oglesby (2009). Evidence from coseismic slip gradients for dynamic control on rupture propagation and arrest through stepovers, *J. Geophys. Res.*, **114**, B02312, doi:10.1029/2008JB005969.
- Field, E. H., T. E. Dawson, K. R. Felzer, A. D. Frankel, V. Gupta, T. H. Jordan, T. Parsons, M. D. Petersen, R. S. Stein, R. J. Weldon II, and C. J. Wills (2009). The uniform California earthquake rupture forecast, version 2 (UCERF 2), *Bull. Seismol. Soc. Am.*, **99**, 2053-2107, doi: 10.1785/0120080049.
- Field, E. H., and M. T. Page (2011). Estimating Earthquake-Rupture Rates on a Fault or Fault System, *Bull. Seismol. Soc. Am.*, **101**, 79–92, doi: 10.1785/0120100004
- Frankel, A. D., M. D. Petersen, C. S. Mueller, K. M. Haller, R. L. Wheeler, E.V. Leyendecker, R. L. Wesson, S. C. Harmsen, C. H. Cramer, D. M. Perkins, and K. S. Rukstales (2002). Documentation for the 2002 Update of the National Seismic Hazard Maps, U. S. Geol. Surv. Open File Rep., OFR-02-420, 33pp.
- Harris, R. A., and S. M. Day (1993). Dynamics of fault interaction: Parallel strike-slip faults, *J. Geophys. Res.*, **98**, 4461-4472.
- Harris, R. A., and S. M. Day, (1999). Dynamic 3D simulations of earthquakes on en echelon faults, *Geophys. Res. Lett.*, **26**, 2089-2092.
- Kase, Y., and K. Kuge (1998). Numerical simulation of spontaneous rupture processes on two non-coplanar faults: the effect of geometry on fault interaction, *Geophys. J. Int.*, **135**, 911-922.
- Lettis, W., J. Bachhuber, R. Witter, C. Brankman, C. E. Randolph, A. Barka, W. D. Page, and A. Kaya, (2002). Influence of releasing step-overs on surface fault rupture and fault segmentation: Examples from the 17 August 1999 Izmit earthquake on the North Anatolian fault, Turkey, *Bull. Seismol. Soc. Am.*, **92**, 19-42.
- Li, H.-B., Wang, Z.-X., Fu, X.-F., Hou, L.-W., Si, J.-L., Qiu, Z.-L., Li, N., Wu, F.-Y. (2008). The surface rupture zone distribution of the Wenchuan earthquake ($M_s8.0$) happened on May 12th, 2008, *Geology in China*, **35**, 803-813.

- Lozos, J. C., D. D. Oglesby, B. Duan, and S. G. Wesnousky (2011). The effects of double fault bends on rupture propagation: A geometrical parameter study, *Bull. Seismol. Soc. Am.*, **101**, 385–398, doi: 10.1785/0120100029.
- McCann, W. R., S. P. Nishenko, L. R. Sykes, and J. Krause (1979). Seismic gaps and plate tectonics: seismic potential for major boundaries, *Pure Appl. Geophys.*, **117**, 1082–1147.
- Okada, Y., Internal deformation due to shear and tensile faults in a half-space, *Bull. Seismol. Soc. Am.*, **82**, 1018–1040, 1992.
- Oglesby, D. (2008). Rupture termination and jump on parallel offset faults, *Bull. Seismol. Soc. Am.*, **98**, 440–447, doi: 10.1785/0120070163
- Petersen, M. D., A. D. Frankel, S. C. Harmsen, C. S. Mueller, K. M. Haller, R. L. Wheeler, R. L. Wesson, Y. Zeng, O. S. Boyd, D. M. Perkins, N. Luco, E. H. Field, C. J. Wills, and K. S. Rukstales (2008). Documentation for the 2008 update of the United States National Seismic Hazard Maps, US Geol. Surv. Open File Rep., 2008-1128, 61pp.
- Romeo, R. W. (2005). Earthquake hazard in Italy, 2001–2030, *Natural Hazards*, **36**, 383–405, doi:10.1007/s11069-005-1939-1.
- Simpson, R. W. and P. A. Reasenber, Earthquake-induced static-stress changes on central California faults, *U. S. Geol. Surv. Prof. Pap. 1550-F*, 55–89, 1994.
- Wesnousky, S. G. (2008). Displacement and geometrical characteristics of earthquake surface ruptures: Issues and implications for seismic-hazard analysis and the process of earthquake rupture, *Bull. Seismol. Soc. Am.*, **98**, 1609–1632, doi: 10.1785/0120070111.
- Working Group on California Earthquake Probabilities (1988). Probabilities of large earthquakes occurring in California on the San Andreas fault, U.S. Geological Survey Open-File Report, 62 pp.
- Working Group on California Earthquake Probabilities (1990). Probabilities of large earthquakes in the San Francisco Bay Region, California, U.S. Geological Survey Circular, 51 pp.
- Working Group on California Earthquake Probabilities (WGCEP) (1995). Seismic hazards in Southern California: Probable earthquakes, 1994 to 2024, *Bull. Seismol. Soc. Am.*, **85**, 379–439.
- Working Group on California Earthquake Probabilities (WGCEP) (2003). Earthquake probabilities in the San Francisco Bay region: 2002 to 2031, USGS Open-File Report 03-214.